Design of Planar Circuit Structures with an Efficient Magnetostatic-Field Solver

Stefan Lindenmeier, *Member, IEEE,* and Peter Russer, *Fellow, IEEE*

***Abstract*— We introduce a highly efficient field solver for the calculation of the quasi-static magnetic field in order to design lossless planar circuit elements with nearly arbitrary shape. The field solver is based on a finite-difference (FD) formulation of a scalar magnetic potential, using potential partitioning surfaces (PPS's). The modeling of the quasi-static fields in distributed circuit elements leads to the development of lumped element equivalent circuits in a very fast and efficient way. For structures with sizes far below the wavelength, the equivalent circuits can be derived in a direct way. For the field modeling of larger structures, the quasi-static field solver can be used in a hybrid full-wave analysis as well. Numerical examples are presented for different planar-circuit elements.**

***Index Terms*— CAD, finite-difference magnetic field, quasi-static.**

I. Introduction

FOR THE design of planar-circuit elements, the given structures are mostly extracted to a lumped element circuit model. In many applications, it is sufficient to divide the circuit structure into conductor elements and substructures, which contain discontinuities and junctions between the conductor elements. While the conductor elements are modeled easily by two-dimensional (2-D) field solvers, the three-dimensional (3-D) field modeling, which leads to high computation effort, has to be done only for the substructures between the conductors. The lumped-element circuits of these structures can be developed efficiently by calculating the quasi-static electric and magnetic fields, because these substructures are far below the given wavelengths. On the other hand, the substructures of the given circuit may have a complicated geometry. With that, a flexible computer-aided design (CAD) tool for the efficient simulation of the quasi-static fields in lossless planar circuit structures of arbitrary geometry is required.

The demand for a method of simulating the field in structures with arbitrary geometry leads to a space discretizing method like the finite-difference (FD) method [1], [2]. The structure of the circuit elements is discretized according to Yee's scheme [2]. For the simulation of the electrostatic field, Maxwell's equations are reduced to a Poisson equation of the electrostatic potential. This reduction of considering only a scalar potential instead of the three components of the electric field leads to considerable savings in computation time and storage. With that, capacitances of various circuit elements are very efficiently calculated.

While the electrostatic field can be calculated in a fast way by means of a scalar potential, the calculation of the magnetic field cannot be directly performed in such a simple way. This is because in contrast to the electric field, the contour integral of the magnetic field does not disappear if a conductor is enclosed. Thus, in general, this would mean to calculate the field in terms of three components which makes the computational effort increase. The law of Biot–Savart cannot be used for the calculation because the current distribution is unknown.

Manuscript received March 31, 1997; revised August 15, 1997.

The authors are with Lehrstuhl für Hochfrequenztechnik, Technische Universität München, 80333 Munich, Germany.

Publisher Item Identifier S 0018-9480(97)08327-0.

II. The PPS-FD Field Solver

In this paper, we present a potential-partitioning-surface finite-difference (PPS-FD) field solver for the efficient simulation of the quasi-static magnetic field in arbitrary lossless planar-circuit structures. Using this method, we can easily calculate the inductances in 3-D structures for generating their lumped-element models.

Compared with an FD full-wave analysis, the simulation of the magnetic field with the PPS-FD solver requires less than 1/20 of the central processing unit (CPU) time and 1/3 of the memory. The solver is also applicable for a hybrid dynamic-static FD method for efficient field simulation in structures of larger size in relation to the wavelength, as has been presented in [3] and [4].

The PPS-FD-solver is based on the introduction of PPS's into the 3-D structure, connecting each conductor in the structure with the outer boundary in a way that each possible integration path around the conducting material crosses the PPS. Fulfilling this requirement, the choice of the exact position of the PPS is arbitrary. Assuming the case of a lossless 3-D structure, the consideration of the field is reduced to the spatial region around the conducting material. This region is cut by the PPS so that the resulting subregion is bordered by two more surfaces which are both sides of the PPS. In this newly defined domain, the magnetic field is irrotational and, hence, it can be described by a scalar magnetic potential M, in analogy to the electrostatic case as follows:

$$\oint_C \mathbf{H}\, d\mathbf{s} = 0 \Rightarrow \mathbf{H} = -\nabla M. \tag{1}$$

For the description of the potential in the subregions, the divergence-free magnetic field yields a simple differential

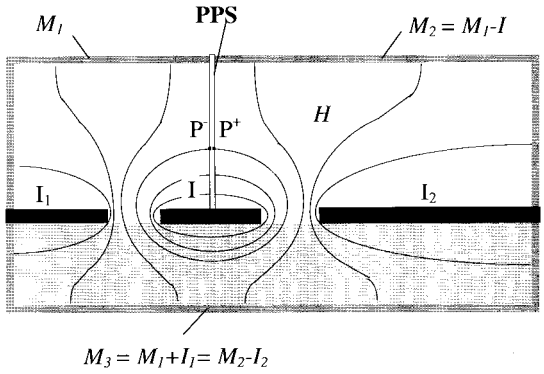

Fig. 1. Example for the incorporation of a PPS into a coplanar structure. Magnetic walls occur as equipotential surfaces with the potentials M_1, M_2, and M_3, which are separated by the PPS and by the metallization.

equation, which leads to a fast numerical algorithm for the calculation of the potential M as follows:

$$\nabla \cdot (\mu \nabla M) = 0. \tag{2}$$

In Fig. 1, the incorporation of a PPS into a coplanar structure is shown. In this example, the structure is defined in a box of magnetic walls.

For monolithic microwave integrated circuit (MMIC) design problems, we assume an ideal skin effect. This means that for the calculation of the quasi-static fields, we define the surface of each metallization as an electric wall in which there exists no normal magnetic-field component.

With that, we derive the following demands for the scalar magnetic potential M at the boundaries. At metallic surfaces (electric walls), the local derivative of the potential in normal direction to a metallization is zero. This enforces the disappearing of the normal magnetic field. Magnetic walls are equipotential surfaces. With that, the tangential magnetic-field components disappear. As can be seen in Fig. 1, the different currents in the conducting material lead to the relating difference between the potentials M_1, M_2, M_3 on the different equipotential surfaces which are separated by the metallization and the PPS.

There are new boundary conditions on the PPS's which are sufficient to describe the influence of the PPS. The integration of the field around a conductor from one side of the PPS to its other side yields a step in potential when passing this PPS. Due to Ampere's law, the integration of the magnetic field from a point P^- on one side of the PPS to the point P^+ on the other side yields the difference of the potentials M at these points (see Fig. 1) [5]. This means that the difference between the potential on one side and the potential on the other side of the partitioning surface is equivalent to the current in the conductor as follows:

$$\int_{P-}^{P^+} \mathbf{H}\, d\mathbf{s} = I \Rightarrow M(P^+) - M(P^-) = I. \tag{3}$$

While the potential M is noncontinuous at the partitioning surface, all the derivatives of M have to be continuous. This results from the requirement that the magnetic-field distribution is independent of the choice of the local position of the PPS at the conductor

$$\mathbf{H}(P^+) = \mathbf{H}(P^-) \Rightarrow \left.\frac{\partial^{l+m+n} M}{\partial x^l \partial y^m \partial z^n}\right|_{P^+} = \left.\frac{\partial^{l+m+n} M}{\partial x^l \partial y^m \partial z^n}\right|_{P-} \tag{4}$$

(for $l, m, n > 0$). Those properties lead to the unique description of the magnetic potential. The calculation of the potential and the magnetic field can now be performed in a fast numerical way.

The differential equation (2) of the potential is realized according to a FD scheme in a Cartesian mesh of elementary cells. The potentials M of the elementary cells are defined on the hyphens of the cells. On the way, the derivatives of first order of M are localized exactly between the potentials of neighboring cells, m is the index of the considered elementary cell. o, r, and h are the index of the neighbored cells in positive x-, y-, z-directions. As an example, a PPS is defined between the cells l and m. The step in potential I is inserted into the corresponding FD term as follows:

$$\begin{aligned} &\overline{\Delta y \Delta z \mu_m} \frac{M_o - M_m}{\Delta x_m} - \overline{\Delta y \Delta z \mu_u} \frac{M_m - M_u}{\Delta x_u} \\ &+ \overline{\Delta x \Delta z \mu_m} \frac{M_r - M_m}{\Delta y_m} - \overline{\Delta x \Delta z \mu_l} \frac{M_m - M_l + I}{\Delta y_l} \\ &+ \overline{\Delta x \Delta y \mu_m} \frac{M_h - M_m}{\Delta z_m} - \overline{\Delta x \Delta y \mu_v} \frac{M_m - M_v}{\Delta z_v} = 0. \end{aligned} \tag{5}$$

According to the FD scheme, the differential equation (2) is applied in form of the linear equation (5) to each mesh cell, combining the potentials of their neighbored cells. With that, the given structure yields a solvable system of equations of this type. The steps in potential at the PPS can be seen as the incorporation of local sources I into the FD system. As with the potentials at magnetic walls, these potential steps can be collected into a source vector in the equation system. The system is then solved numerically, analogous to the FD description system for the electrostatic field. The solution of the magnetostatic system of equations yields a vector in which all the potentials M of the structures cells are included. After that, the magnetostatic field can be determined by the FD quotient of the magnetic potential distribution according to (1).

III. Numerical Results

In the following, we present numerical results of the PPS-FD solver. The PPS-method has been realized in form of a Fortran program and is compared to an FD-full-wave analysis.

In a first example, we consider the magnetostatic field in a coplanar spiral inductor on silicium substrate. As is shown in Fig. 2, the PPS connects the spiral conductor vertically to the ground plane. The conductor route leading to the center of the

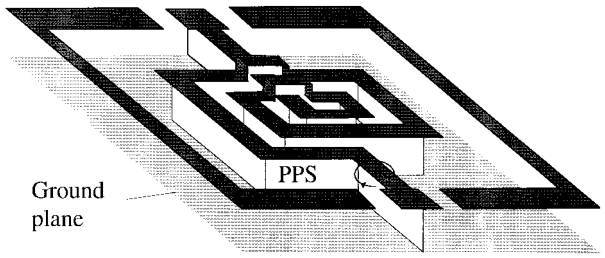

Fig. 2. The incorporation of a PPS into a coplanar spiral structure.

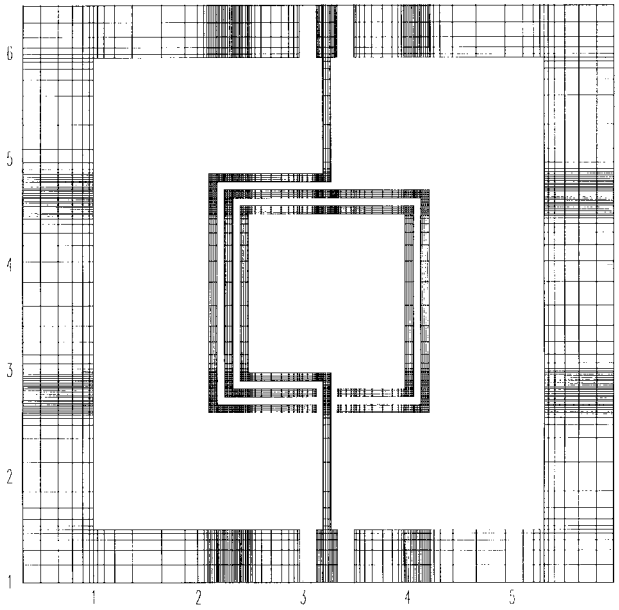

Fig. 3. Coplanar spiral inductor with two air bridges, presentation in the spiral plane.

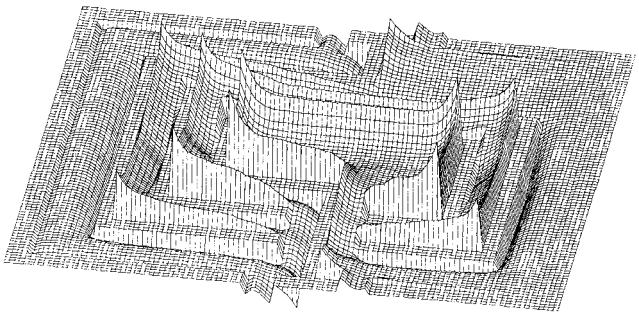

Fig. 4. Field H_x of the spiral inductor, presented in the spiral plane.

spiral is crossed by the spiral in the form of two air bridges. By following the spiral route, the PPS crosses itself below the air bridges. In Fig. 3, we see the spiral structure with its discretization steps. The discretization in the inner space is not shown in this figure. In Fig. 4, the H_x component in the spiral plane is shown, which is numerically obtained by the PPS-FD solver. Fig. 5 shows the H_x component in a plane 10 μm below the spiral plane. Though this plane is cut by the PPS, no discontinuities in the field distribution can be seen. This proves that the numerically computed magnetic field is independent of the PPS position as it is necessary on physical reasons.

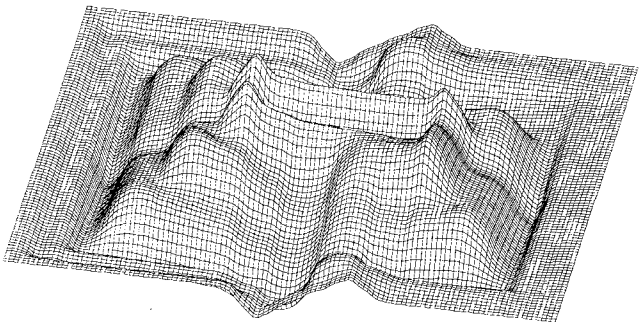

Fig. 5. Field H_x in the spiral inductor, 10 m below the spiral plane.

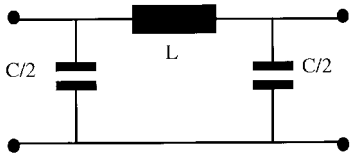

Fig. 6. Lumped-element equivalent-circuit model of the spiral structure in the frequency range of $\Omega_C \ll 1/\Omega_L$.

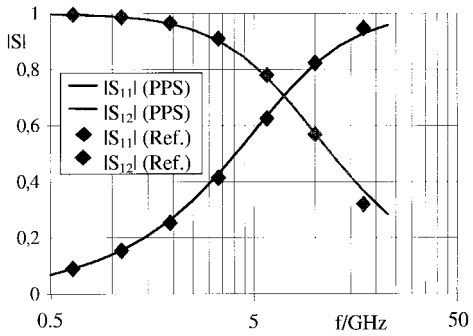

Fig. 7. Absolute values of S_{11} and S_{12} calculated by the PPS-method, accurate reference solutions calculated by an FDFD.

The structure is discretized into half-a-million mesh cells. For comparison, the computation of the magnetic filed with a FD full-wave analysis in frequency domain (FDFD) requires approximately 40 h CPU time on a DEC 3000/800 Alpha workstation. In contrast to the full-wave analysis, the PPS-FD solver requires only approximately 1 h for the magnetostatic field of the spiral structure. This is the same low computational effort as for the analysis of the electrostatic field. Thus, by using the PPS-FD solver for extracting the low-frequency lumped-element model of the spiral structure, we have a reduction in computation time to 2.5%. With higher cell numbers there would even be a higher reduction. The required storage is reduced to 33%.

We derive the lumped-element parameters of the equivalent-circuit model of the spiral structure, as is shown in Fig. 6. It is sufficient for the description of the circuit characteristics in the frequency range of $\omega C \ll 1/\omega L$.

By choosing electric walls at the gates of the spiral structure, we realize a short circuit at the gates. The excitation of the field is done by implementing a step in potential at the PPS. After calculating the quasi-static magnetic-field, the inductance of the spiral structure is easily calculated by calculating the magnetic flux Φ. It is derived by integrating the normal

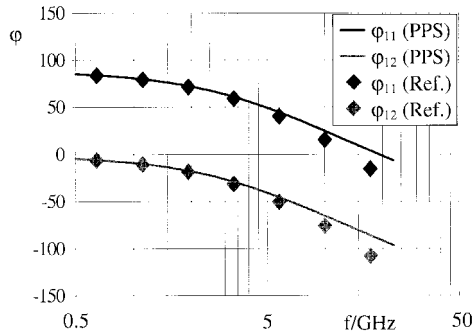

Fig. 8. Phases j of S_{11} and S_{12} calculated by the PPS-method, accurate reference solutions by FDFD analysis.

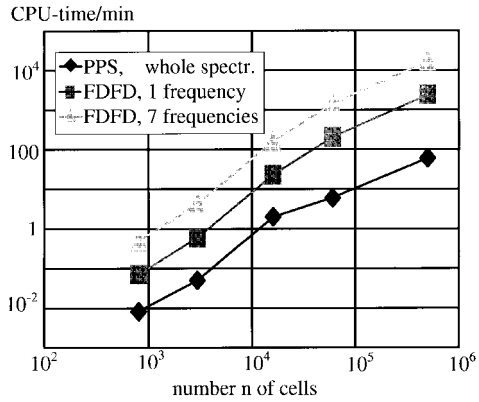

Fig. 9. CPU time of field simulations in dependence of the number n of cells of the discretization. Comparison of the PPS and the FDFD method (Data produced on a DEC 3000/800 Alpha workstation).

magnetic-field component along the PPS. This is because all flux lines which surround the conductor are passing the PPS. In case of the spiral structure, we obtain the inductance $\Phi/I = 2.46$ nH.

For the calculation of the capacitance C, an open circuit at the gates is realized by choosing magnetic walls at the gates. The capacity of the structure is derived by integrating the normal quasi-static electric field along the surface of the metallization.

From the equivalent-circuit model we derive the S-parameters which are shown in Figs. 7 and 8. They are compared to the S-parameters which were calculated by the FDFD full-wave analysis with 40 times higher computation time. As can be seen, the S-parameters in the frequency range up to 5 GHz are of very good agreement in phase and absolute value. It is obvious that the results approximate to each other only under the condition that time delay of the waves in the spiral structure has no considerable influence. As can be seen, the results are of good agreement in the frequency range up to 5 GHz. In this frequency range, the wavelength is more than ten times higher than the length of the spiral inductor.

For estimating the efficiency of the PPS method, we compare the computation times between the PPS method and the FD full-wave analysis. For the comparison we use the same discretization for the simulations with both methods.

Fig. 9 shows the CPU time of the methods in dependence of the number of cells which were used for the simulations. The

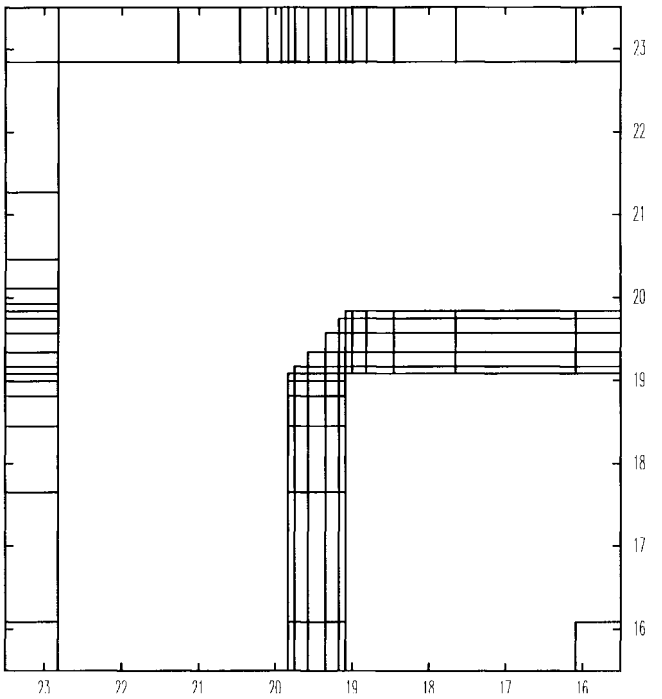

Fig. 10. Microstrip bend with edge compensation, presentation in the microstrip plane (all sizes in 100 μm).

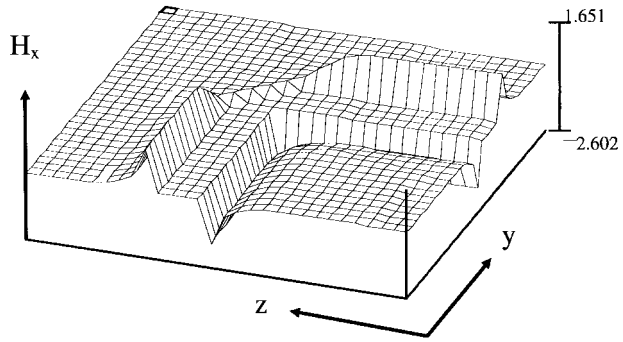

Fig. 11. Field H_x of the microstrip bend in the microstrip plane.

CPU time of the PPS simulations is more than one decade lower than the CPU time of the FDFD simulations. Additionally, it is also increasing more slowly with an increasing number n of cells for the discretization. This means that the benefits of the PPS method are increasing with the demand of a higher accuracy in the calculations.

The comparison of the PPS method with the conventional FDFD method shows that the efficiency of the PPS method is considerably higher due to the high reduction in computation time. This is true also for the storage which is related to the mesh size n. Due to sparsity, the matrix size of both the conventional and hybrid approach grows linearly with n. However, due to the simplified mathematics in the static case, this type of analysis consumes only 33% of the corresponding full-wave problem.

As a further example, we consider a microstrip bend $(Z_c = 50\ \Omega)$ with edge compensation, as can be seen in Fig. 10. The PPS is again connecting the microstrip conductor to the ground plane. While the distance of the microstrip line to the ground

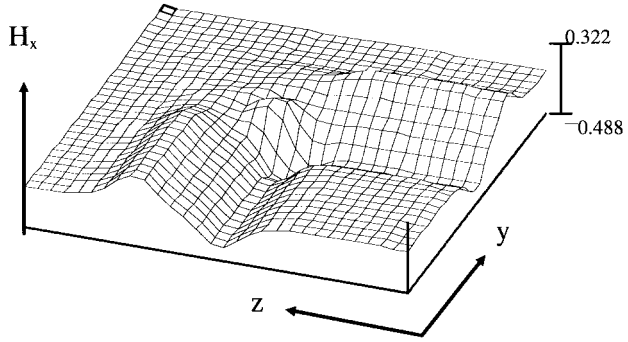

Fig. 12. Field H_x of the microstrip bend, 15 m below the microstrip plane.

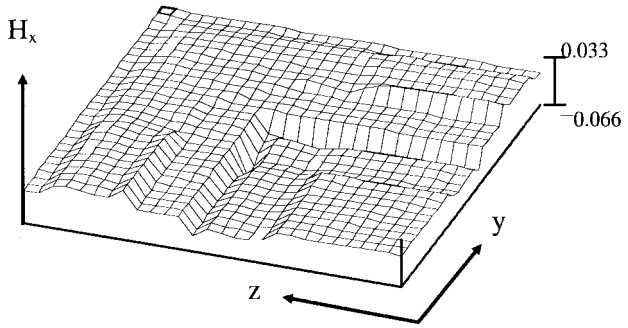

Fig. 13. Field deviations ΔH_x between the field of the symmetrical and unsymmetrical microstrip bend in the microstrip plane.

plane is 100 μm, the distance of the line to the upper boundary of the box is 500 μm. Fig. 11 shows the calculated magnetostatic field of the structure in the microstrip plane. Fig. 12 shows the calculated field 15 μm below the microstrip plane.

For further verification of our results, we also calculated the magnetostatic field for a triplate bend with edge compensation, which is identical to the microstrip bend of Fig. 10, but with symmetry to the x-axis. The magnetic field in this structure can be easily calculated according to a method in [6], which also uses a scalar potential. This method has the same high efficiency, but is restricted to nearly symmetrical structures. It is assumed that the field is nearly symmetrical to the metallization plane. We now compare the results of the PPS method to results of the method of [6] investigating the same computation effort. Without using PPS, this method is only restricted to structures of approximate symmetry to the metallization plane like the triplate structure. In this case, the results of the methods were nearly identical with a relative difference of 10^{-6}%. While the accuracy of the PPS method is not dependant of the structure's geometry, the assuming of a symmetric field for the unsymmetric microstrip bend would lead to an unacceptable field deviation, as can be seen in Fig. 13.

The S-parameters of the microstrip bend were obtained by calculating the lumped-element parameters of the equivalent-circuit model, as shown in Fig. 14. This model is sufficient for the frequency range of $\omega C \ll 1/\omega L$. In Fig. 15, the absolute value of the S_{11}-parameter is shown. The results are compared to accurate simulation results by use of an FD full-wave analysis. The deviations of the results are lower than 2% in the whole frequency range. In the range of higher frequencies,

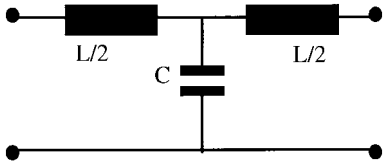

Fig. 14. Lumped-element equivalent-circuit model of the microstrip bend in the frequency range of $\omega C \ll 1/\omega L$.

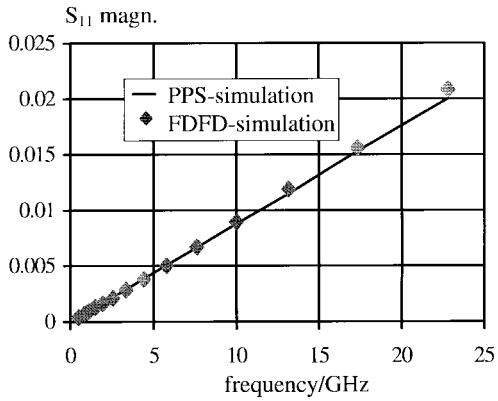

Fig. 15. Absolute values of S_{11}, calculated by the PPS method, reference solutions by FD full-wave analysis.

the approximation of a quasi-static field again leads to a little increase of the deviations.

IV. Conclusion

We present a highly efficient PPS-FD solver for the fast calculation of the magnetostatic field. The PPS method leads to the calculation of a well-defined scalar magnetic potential. It is applicable without restriction to all types of lossless 3-D structures. Using the PPS, the numerical effort for the FD calculation of the quasi-static magnetic field is as low as for the electrostatic field. Compared to the FD method in frequency domain, the effort on CPU time for the magnetic-field simulation is reduced to less than 1/20, and the storage requirement decreases to 1/3. The PPS method can be used for calculating inductances and for the application in a hybrid dynamic-static FD method.

References

[1] S. Yee, "Numerical solution of initial boundary value problems involving Maxwell's equations in isotropic media," *IEEE Trans. Antenna Propagat.*, vol. 14, pp. 302–307, May 1966.

[2] T. Weiland, "On the numerical solution of Maxwellian eigenvalue problems in three dimensions," *Particle Accelerators*, vol. 17, pp. 227–242, 1985.

[3] S. Lindenmeier, P. Russer, and W. Heinrich, "Hybrid dynamic-static finite-difference approach for MMIC design," in *Int. Microwave Symp. Dig.*, vol. 1, San Francisco, CA, June 1996 pp. 197–200.

[4] S. Lindenmeier, P. Russer, and W. Heinrich, "Applications of the hybrid dynamic-static finite difference approach on 3D-MMIC structures," presented at the *Progress Appl. Computational Electromagnetics ACES Symp.*, Monterey, CA, Mar. 1997.

[5] J. Simonyi, "Theoretische Elektrotechnik," *Hochschulbücher der Physik*, vol. 20. Berlin, Germany: Verlag, 1979.

[6] M. Abdo-Tuko, M. Naghed, and I. Wolff, "Novel 18/36 GHz (M)MIC GaAs FET frequency doublers in CPW-techniques under the consideration of the effects of coplanar discontinuities," *IEEE Trans. Microwave Theory Tech.*, vol. 41, pp. 1307–1315, Aug. 1993.

Stefan Lindenmeier (M'97) was born in Munich, Germany, in 1967. He received the Dipl.-Ing. and the Dr.-Ing. degrees from the Technical University of Munich, Munich, Germany, in 1994 and 1996, respectively, both in electrical engineering.

From 1994 to 1996, he was with the Computer-Aided Design Department, Ferdinand Braun Institut Berlin, Berlin, Germany where he worked on numerical techniques for the field-theoretical analysis of microwave circuits. In 1996, he joined the Lehrstuhl für Hochfrequenztechnik at the Technische Universität München, Munich, Germany, as an Assistant Professor. His current research interests are the development and application of CAD tools for the analysis of EMC problems, MMIC, and antenna design.

Peter Russer (SM'81–F'94) was born in Vienna, Austria, in 1943. He received the Dipl. Ing. and the Dr. Techn. degrees from the Technische Universität, Vienna, Austria, in 1967 and 1971, respectively, both in electrical engineering.

From 1968 to 1971, he was an Assistant Professor at the Technische Universität in Vienna. In 1971, he joined the Research Institute of AEG-Telefunken, Ulm, Germany, where he worked on fiber-optic communication, broad-band solid-state electronic circuits, statistical noise analysis of microwave circuits, laser modulation, and fiber-optic gyroscopes. Since 1981, he has held the chair of Hochfrequenztechnik at the Technische Universität München. From October 1992 to March 1995, he also has been the Director of the Ferdinand-Braun-Institut für Hchstfrequenztechnik, Berlin, Germany. His current research interests are integrated microwave and millimeter-wave circuits, electromagnetic fields, statistical noise analysis of microwave circuits, and methods for computer-aided design of microwave circuits. He has authored over 200 scientific papers in these areas.

Dr. Russer is a member of the German Informationstechnische Gesellschaft and the Austrian and German Physical Societies. He was co-recipient of the NTG Award in 1979.